Received: 8 July 2020 | Revised: 21 November 2020 | Accepted: 5 December 2020

DOI: 10.1002/pip.3387

EU PVSEC PAPER

PROGRESS IN PHOTOVOLTAICS WILEY

Industrialization of hybrid Si/III–V and translucent planar micro-tracking modules

Gaël Nardin[1] | César Domínguez[4,5] | Álvaro Fernando Aguilar[1] | Laetitia Anglade[1] | Mathilde Duchemin[1] | David Schuppisser[1] | Florian Gerlich[1] | Mathieu Ackermann[1] | Laurent Coulot[1] | Blaise Cuénod[2] | Delphine Petri[2] | Xavier Niquille[3] | Nicolas Badel[2] | Agata Lachowicz[2] | Matthieu Despeisse[2] | Jacques Levrat[2] | Christophe Ballif[2,3] | Stephen Askins[4] | Rubén Núñez[4] | Norman Jost[4] | Guido Vallerotto[4] | Ignacio Antón[4]

[1]Insolight SA, Ecublens, Switzerland

[2]CSEM SA, PV-Center, Neuchatel, Switzerland

[3]Photovoltaics and Thin-Film Electronics Laboratory, Institute of Microengineering (PVLAB), Swiss Federal Institute of Technology Lausanne, Lausanne, Switzerland

[4]Instituto de Energía Solar, Universidad Politécnica de Madrid, Avda. Complutense, 30, Madrid, 28040, Spain

[5]Escuela Técnica Superior de Ingeniería y Diseño Industrial, Universidad Politécnica de Madrid, Madrid, Spain

Correspondence
César Domínguez, Instituto de Energía Solar, Universidad Politécnica de Madrid, Madrid, Spain.
Email: cesardd@ies.upm.es

Funding information
H2020 Science with and for Society, Grant/Award Number: 787289 grant, project GRECO; H2020 Societal Challenges, Grant/Award Number: 857775 grant, project HIPERION; Innosuisse - Schweizerische Agentur für Innovationsförderung, Grant/Award Number: Helios; Eurostars Program, Grant/Award Number: MEPV2

Abstract

A tracking-integrated hybrid micro-concentrator module is presented that can harvest direct, diffuse, and albedo irradiance components. It uses biconvex 180× lens arrays to concentrate direct light on high-efficiency III–V solar cells (29% module efficiency has been demonstrated outdoors on direct sunlight at Concentrator Standard Test Conditions) and a planar micro-tracking mechanism to allow installation in static frames. Two architectures have been developed to harvest diffuse irradiance: (1) a hybrid architecture where the backplane is covered with monofacial or bifacial Si cells; (2) a translucent architecture where diffuse light is transmitted through the module for dual-land-use applications, such as agrivoltaics. Simulations show that the hybrid architecture provides an excess of yearly energy production compared to 20% efficiency flat-plate photovoltaic (PV) module in all locations studied, including those with a low direct normal irradiance (DNI) content, and up to 38% advantage in high-DNI locations. The use of bifacial heterojunction and interdigitated back-contact Si cells has been explored for the glass–Si–glass backplane laminate to harvest albedo light. Bifacial gains modeled can boost energy yield by about 30% in the best scenario. We discuss the perspectives of the translucent modules for dual-land-use applications as well, such as integration in greenhouses for agriculture-integrated PV (agrivoltaics). This architecture can provide up to 47% excess electricity compared to a spaced reference Si array that transmits the same amount of solar

photosynthetically active radiation for crop production. The HIPERION consortium funded by the European H2020 program is making an intensive effort to take this technology to the industrial scale.

KEYWORDS
agrivoltaics, agrophotovoltaics, bifacial silicon, hybrid PV module, III–V concentrator, micro-concentrator, static concentrator, tracking-integrated concentrator

1 | INTRODUCTION

Despite having achieved the largest photovoltaic (PV) conversion efficiency to date (Steiner et al,[1] p. 43), concentrator photovoltaics (CPV) has not yet been able to compete with silicon flat-plate because of higher investment costs and a potential market limited to utility-scale projects in locations with a high fraction of direct sunlight.[2] Furthermore, the need of bulky two-axis trackers prevents their use in rooftop installations. For some years now, research groups around the world have been intensively exploring some innovations to overcome these difficulties, notably

- Micro-scale concentrating photovoltaics: reducing cell size below 1 mm to introduce fundamental gains, notably the reduction of light absorption, thermal losses, material consumption, and carbon footprint.[3]
- Integrated tracking: the module chassis remains static while sunlight is concentrated on the cells via some internal tracking mechanism.[4] This allows installing the module on a fixed structure and enables CPV for residential or commercial rooftop markets.
- Use of the diffuse fraction: conventional CPV systems can only capture direct sunlight, which strongly affects their market opportunities as the diffuse fraction accounts for 10% to 30% of total insolation even in high direct normal irradiance (DNI) areas.[5] The diffuse irradiance is transmitted by the primary optics but spread over the back plane rather than concentrated on the III–V solar cells. The diffuse irradiance can either be harvested by large non-concentrator PV cells (e.g., Si or thin film) installed on the backplane, thus creating a dual or hybrid CPV/flat-plate module, or transmitted through the module for dual-land-use applications.

The Swiss start-up Insolight has developed a micro-CPV module based on high-efficiency III–V multi-junction solar cells that incorporates planar micro-tracking and a hybrid CPV/flat-plate architecture. Integrated tracking enables fixed-mount rooftop applications and the hybrid approach makes the concept suitable for locations with a high diffuse fraction. After the demonstration of a module efficiency of 29%, the HIPERION consortium funded by the European H2020 program is making an intensive effort to take this technology to the industrial scale. Based on a similar planar tracking architecture, Insolight is also developing translucent modules that transmit diffuse light and open up perspectives for integration in buildings (BIPV) or dual-land-use applications (e.g., agrivoltaics). This work presents the main design concepts behind these technologies, the challenges in the roadmap to commercialization and the ongoing efforts for accurately modeling its performance in order to estimate the energy yield gains that can be achieved with respect to conventional flat-plate modules.

2 | INSOLIGHT'S PLANAR MICRO-TRACKING MODULE WITH DIFFUSE LIGHT HARVESTING

There are two fundamental approaches to integrate tracking within a module: beam steering and micro-tracking.[4] In the former, the varying incidence angle of sunlight is redirected towards the concentrator optics through the mechanical movement of some steering element (like a prism or a mirror) or by varying its optical properties. In the micro-tracking approach, the light is concentrated by the optical layer into some particular location, which changes with varying solar angles, and then some internal tracking element moves the solar cell or a coupling element to capture this concentrated light. This approach needs a special optical design to ensure high concentration for the wide range of angles of incidence (AOIs) of daily direct sunlight, as the focal length of a lens varies with AOI.[6] Therefore, lateral and vertical adjustments to the receiver plane (solar cells) are needed to track the sun. Insolight has developed a planar tracking mechanism able to transform lateral actuation into lateral and vertical displacements. Other mechanisms that pursue the same objective have been published in the literature.[7,8] The planar micro-tracking enables Insolight modules to be installed at a fixed tilt in a static frame (Figure 1A). Direct sunlight is focused by a polymer lens array onto III–V triple-junction cells with a concentration factor of 180×. As the sun moves across the sky, the spots of concentrated light have to be captured by the cells, so a planar micro-tracking mechanism shifts the backplane with respect to the optics and the chassis to track the sun for AOIs up to 55° (Figure 1B). This tracking range can be sufficient to collect roughly 80% of the yearly irradiation available in installations without near-field shadows. However, this figure is increased in urban landscapes because steep incidence angles are often intercepted by buildings nearby.

To ensure optimal concentrating power and transmission over a wide range of AOIs, a biconvex aspheric lens design is proposed, similar to others described in the literature.[8] Fresnel lenses or other plano-convex designs have been excluded due to their poor off-axis performance. The aspherical coefficients of the biconvex lens were

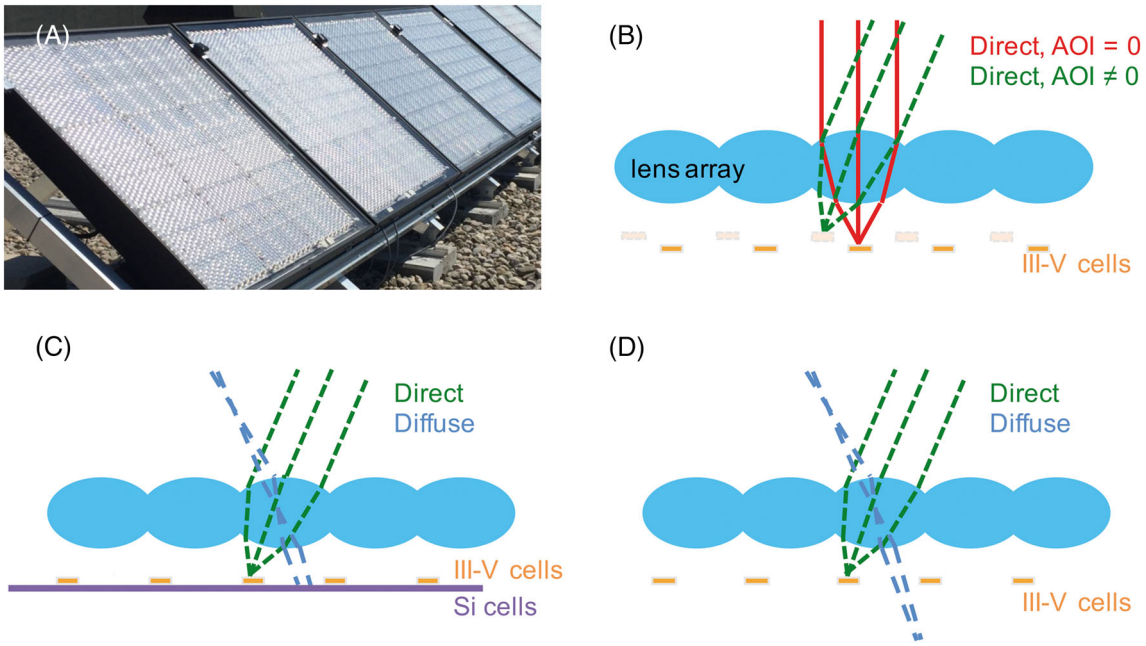

FIGURE 1 (A) Photograph of the Insolight pilot site on a rooftop of the EPFL campus in Lausanne, Switzerland. (B) Simplified sketch of Insolight's planar micro-tracking system. The III–V cell array is translated with respect to the lens array to accommodate for different angles of incidence (AOIs) of the direct sunlight. (C) Sketch of the hybrid Si/III–V architecture where diffuse light is captured by Si cells. (d) Sketch of the translucent architecture where diffuse light is transmitted through the back plane

optimized for optical efficiency and angular tolerance using ray-tracing simulations. Hexagonal lens tiling is chosen to minimize vignetting by the lens edges. The angular performance of the optical system is detailed in Section 3.1. A first laboratory prototype with seven cells achieved a direct sunlight conversion efficiency of 36.4% in 2016.[9,10] A pilot site is installed since 2017 at the rooftop of EPFL, Switzerland (Figure 1A) to validate the robustness of the module architecture and tracking mechanism.[10] In 2019, a 0.1-m^2 pre-series module was characterized with a 29.0% efficiency at Concentrator Standard Test Conditions (CSTC, as defined in IEC 62670-1). In order to increase angular tolerances to manufacturing errors, a secondary glass half-ball lens was attached to the solar cells. This module already featured a tracking range of ±55°.[11] The dominating loss factors from the lab prototype to the pre-series module are (1) optical losses due to the addition of a protection glass and (2) alignment losses.

In conventional CPV systems, diffuse sunlight is wasted as it does not get focused on the solar cells due to limited angular acceptance of concentrator optics. This loss strongly affects their market opportunities, as the diffuse fraction is in the range of 10% to 30% even in locations with a high DNI, and a fraction of 40% is easily found in populated areas.[5,12] Insolight has developed two different architectures to harvest diffuse sunlight:

A. A hybrid CPV/PV architecture (Figure 1C) where diffuse light spread over the back plane is captured by large flat-plate Si cells behind the III–V concentrator cells.
B. A translucent architecture (Figure 1D) where diffuse light is transmitted through the module for dual-land-use applications

Furthermore, the ability to capture diffuse light reduces the sensitivity to soiling of CPV optics, which generates losses that depend on the location and plant maintenance protocols.[13] In a hybrid or translucent module, forward-scattered light from dust particles that is not concentrated on the III–V solar cells is transmitted to the back plane where it can be harvested by flat-plate Si cells or allowed to escape through.

2.1 | Hybrid III–V/Si architecture

In the CPV-on-PV architecture, direct sunlight is focused on the high-efficiency III–V triple-junction cells, while diffuse light, transmitted through the optical layer, is captured by a layer of lower cost Si cells, as shown in Figure 1C. The concept enables extension of planar-micro-tracking CPV to locations with lower DNI content, as it approaches the efficiency of Si panels under diffuse illumination conditions, and provides an efficiency boost in case of direct illumination. The perspective has motivated several groups to explore the idea in various realizations: III–V cells located in-between spaced Si cells,[14] mounted on a transparent substrate above the Si cells,[14–16] or directly mounted on top of the Si cell.[5,12,17,18] Hybrid Insolight modules initially took the first approach. The aspherical coefficients that define the shape of the biconvex lens were optimized using ray-tracing simulations in order to maximize simultaneously the amount of direct light concentrated on a 1-mm triple-junction cell and the amount of diffuse light transmitted and captured by the flat-plate Si cells. The c-Si cells were laser-ablated to create holes where the III–V cells were

installed.[10] The Si cells captured successfully the diffuse radiation but also recovered a significant fraction of the direct light for AOIs larger than the tracking range, which would otherwise be lost (Figure 2). However, the assembled modules also revealed limitations of the laser-ablated Si cells: reliability issues (delamination of the Si cells near the holes), fill factor drop (leading to a poor efficiency of 7.5% for the Si cells) attributed to short circuits created by the ablation, and prohibitive processing costs for industrialization perspectives.

In order to overcome these limitations, a new process was implemented where the III–V cells are assembled on a glass substrate, which can then be integrated within a glass–Si–glass laminate (Figure 3). This approach benefits from the maturity of the standard glass–Si–glass laminates in terms of reliability and cost. Moreover, the laminate is compatible with bifacial Si cells, which can capture albedo from the surroundings. The benefits of using bifacial Si cells in a hybrid CPV/PV architecture were discussed by Martínez et al.[17] The energy gains associated will be further discussed in Section 3.3.

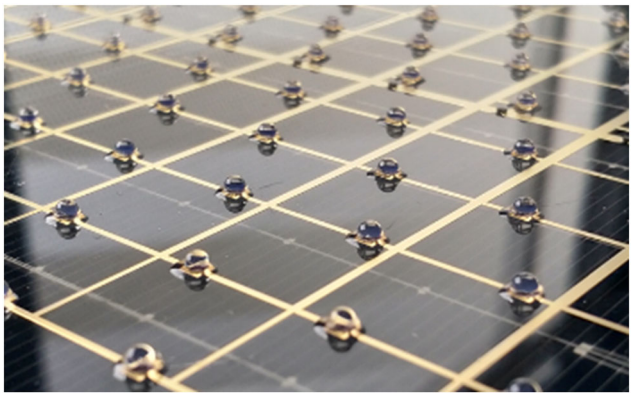

FIGURE 3 Photograph of the backplane of the glass–Si–glass laminate for the Insolight III–V/Si hybrid architecture: III–V cells are assembled on a transparent printed circuit board, which is laminated on top of Si cells (multi-busbar PERC cells in this case, although several alternatives have been studied). III–V cells are encapsulated under secondary optics (half-ball lenses) to increase alignment tolerances

2.2 | Translucent architecture

A second option to utilize diffuse light is to let it be transmitted through the module and use this energy for some other purpose. Diffuse light can be transmitted by assembling the III–V cells on a transparent backplane. The concept has been demonstrated using CPV modules with two-axis tracking.[19,20] It enables CPV applications in building-integrated PV (e.g., skylights) or a dual use of the land on which the PV system is installed, like in the combination with agricultural production (agrivoltaics or agrophotovoltaics). Agrivoltaics is attracting growing attention, and several groups have demonstrated win–win situations or larger-than-unity land use. A pilot study in southern Germany demonstrated a 60% increase of land usage: 80% of electricity produced and 80% of food production.[21] Furthermore, the shading provided by PV systems has been proved beneficial for crop production in eco-systems where water scarcity is an issue.[22]

The most mature implementations are based on spaced Si modules installed on elevated racks[23–25] while technical innovations have explored the integration in greenhouse rooftops of semi-transparent modules based on micro-solar cells,[26] bifacial modules,[27] or wavelength-selective luminescent absorbers.[28] The dynamic control of sunlight on crops via tracking PV modules is also a recent topic of interest, which has been shown to increase crop productivity compared to stationary PV while increasing the ground coverage ratio.[29] When combined with a transparent glass backplane, the planar microtracking of Insolight modules can be used to perform this dynamic control. Tracking can be optimized for instance to ensure sufficient transmitted light at the beginning and the end of the growth season, thus increasing crop yields. Insolight has developed an alternative module architecture with a transparent backplane called Translucent High-Efficiency PV modules for Integration in Agriculture (THEIA, see

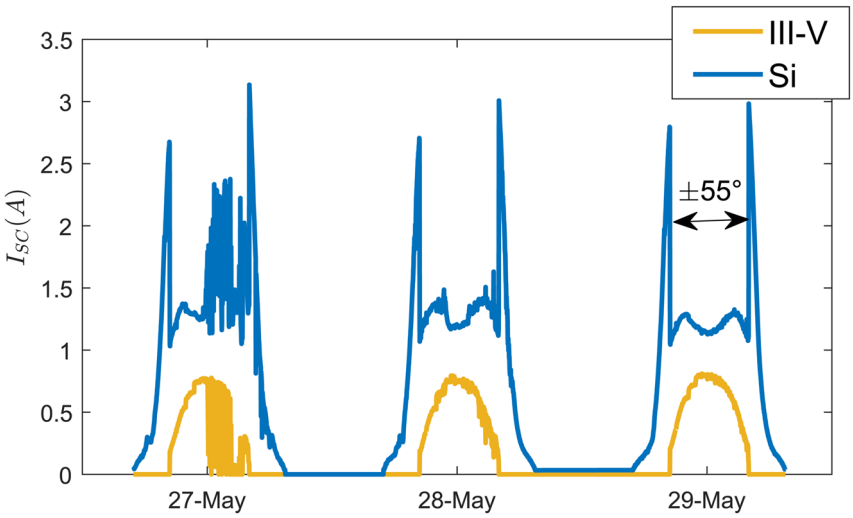

FIGURE 2 Short-circuit current of CPV (III–V) and PV (Si) submodules monitored at the rooftop of the solar energy Institute in Madrid in 2019 during three different types of days with high DNI: afternoon cloud passages (May 27), high-altitude thin clouds (May 28), and clear sky (May 29)

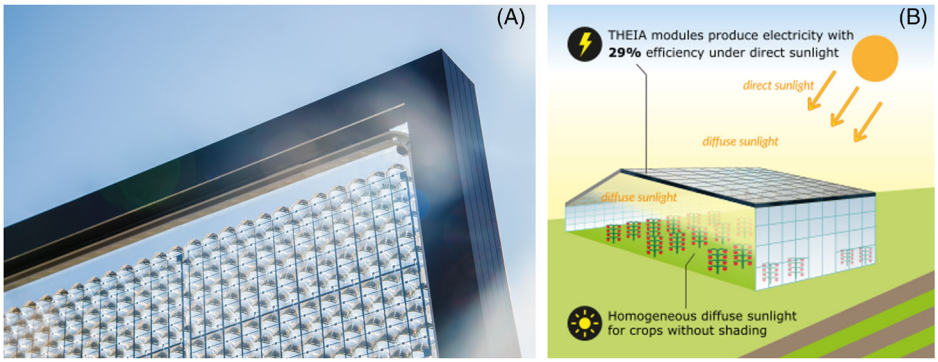

FIGURE 4 (A) Photograph of an assembled planar micro-tracking translucent PV module. (B) Sketch of THEIA modules integrated in the roof of a greenhouse: direct irradiance is converted into electricity and diffuse light is evenly transmitted to the crops below

Figure 4A) to enable this type of applications. Its planar tracking has other potential advantages for agrivoltaics compared to conventional Si panels.[30] The inherent splitting of the direct/diffuse light by CPV optics combines high-efficiency electricity generation from direct light and homogenous illumination of the crops by transmitting diffuse irradiance through. The fixed tilt enables integration in static structures such as the roof of greenhouses, without the need of module spacing (Figure 4B). The lens array acts as a light diffuser that eliminates shadows created by direct light. Previously published calculations predict the energy yield of planar-tracking micro-CPV modules to be similar to conventional, opaque flat-plate Si arrays, while the former additionally provides sufficient photosynthetically active radiation (PAR) for crops.[30] In the next section, we detail further predictions for energy yield and transmitted light.

3 | PERFORMANCE MODELING OF INSOLIGHT TECHNOLOGY

The outdoor characterization of pre-commercial Insolight's hybrid III–V/Si modules presented elsewhere validated their capabilities of diffuse capture, planar micro-tracking, and high direct light-conversion efficiency of nearly 30% CSTC.[11] However, a fundamental step for marketability is the ability to predict energy yield for potential installations at any given site with low uncertainty, in order to provide confidence to investors and project planners. The fundamental gains of the Insolight approach come from non-standard features that cannot be directly modeled with standard PV simulation programs like PVSYST. Insolight has developed performance models that capture the unique behavior of their system and provide energy yield estimations for the different system configurations described above. Due to the rising interest on the hybrid CPV/PV approach and in order to provide the research community or project planners with well-documented and transparent tools to model this type of systems, UPM has created new modules for the open-source library PVLIB Python. Furthermore, CSEM has extended performance models to account for the energy gains linked to the use of bifacial cells for the flat-plate submodule, which are very sensitive to albedo.

3.1 | Insolight performance models and energy yield estimations

In order to estimate the annual energy yield of their modules, Insolight has developed a methodology detailed in this section, which is based on the following steps:

1. Ray-tracing simulation of the lens is used to calculate direct-light-on-III–V and diffuse-light-on-Si effective optical efficiency as a function of the AOI. Reference spectrum is used as input. The external quantum efficiency (EQE) of III–V triple-junction and Si cells is used to estimate their photogenerated currents, respectively.
2. Angular binning of the available yearly irradiation, considering direct and diffuse separately.
3. Calculation of the overall module yield by combining yearly angular distribution bins with the lens performance from Step 1.

3.1.1 | Lens performance

The ability of a PV module to collect light depends on the AOI, primarily because the reflectance and the absorption of the light at the optical layers depends on the effective thickness of the optical layers and the separation between them. This makes sensitivity of module power to AOI higher than that of the cosine response. This effect is typically accounted for by defining an incidence angle modifier (IAM). Standard physical or empirical models found in the literature based on the optical layers of PV modules cannot be used because of the very different characteristics of CPV optical systems. This curve has been characterized using ray-tracing simulations for the two submodules in the Insolight hybrid system (III–V and Si cells). The optical efficiency of the optical system for direct light was simulated as a function of the AOI. Two different lens materials were considered: optical silicone and PMMA, which affects dispersion and spectral absorption properties. Figure 5 plots the angular performance of the biconvex lens for the two materials. For concentration onto the III–V triple-junction cell, optical efficiency is defined as the ratio

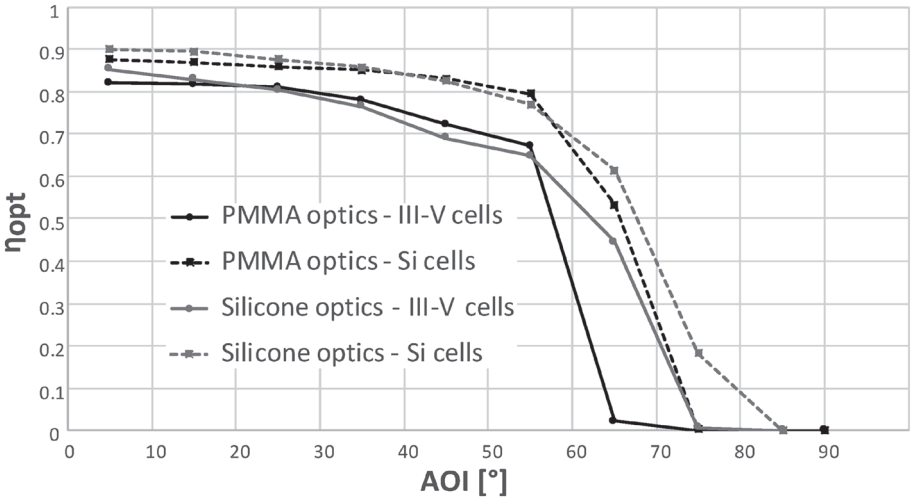

FIGURE 5 Angular performance of the lens design: optical efficiency as a function of AOI for concentration onto a III–V cell (continuous lines) and for light transmission to a Si cell (dashed lines). Two optical designs are shown: silicone lens design (gray lines) and PMMA lens design (black lines)

$$\eta_{\mathrm{opt,III-V}} = I_{\mathrm{III-V}} / I_{0,\mathrm{III-V}},$$

where $I_{0,}$III–V is the photocurrent that the III–V cell would produce if the totality of the light intensity impinging on the lens area would enter the solar cell and *I*III–V is the photocurrent produced by the triple-junction cell under the light concentrated by the designed lens (perfectly aligned, taking into account reflection and absorption losses). The light incident on the lens has a reference AM1.5 direct spectrum (as per ASTM G173-03). The solar cell considered is a triple-junction GaInP/GaInAs/Ge cell. The photocurrent is estimated through the integration of the EQE of each sub-cell with the absorbed spectrum, and taking the minimum of the three sub-cell currents. For the capture of the diffuse light* by c-Si cells, optical efficiency is defined in the same way as for the III–V cells, except that the EQE of a generic c-Si cell is used and the cell dimension is infinite (no concentration losses). For the prediction of transmitted light through the module for crop production, we also used ray tracing and calculated the transmission of the PAR spectrum (400 to 700 nm).

3.1.2 | Direct and diffuse light modeling

Solar radiation data was obtained from the hourly resolved typical meteorological years (TMY) available at the Photovoltaic Geographical Information System (PVGIS) tool,[31] using the long-term average of the 2006–2015 period. From DNI and solar position data, we calculate a polar plot of direct inclined irradiance (DII) for the chosen tilt of the solar panel (see Figure 6, bottom left). The polar plot of diffuse irradiance projected on the panel is calculated from DNI and global horizontal irradiance (GHI) data using a decomposition in 15 sky types (Figure 6, bottom right), as described in Darula and Kittler ,[32] which takes into account local prevailing conditions. The polar plots of direct and diffuse irradiance are then projected in the module plane and binned as a function of AOI (Figure 7). Bins of ±5° are chosen around the AOI values of 5°, 15°, … 85°. These angular distributions are then combined with the optical performance of the system (shown in Figure 5) to integrate the yearly energy yield production.

3.1.3 | Energy yield calculations

The energy yield calculations are based on the angular irradiance and optical efficiency data described above (PMMA optics). The efficiency of the PV and CPV components is calculated on the lens area. The fraction of the module area that is not covered by lenses (e.g., on the edges of the panel) is ignored, as it depends on the module size (decreasing with module size). The system is modeled based on realistic parameters of the Insolight modules: (1) the lens layer is protected by a cover glass (low-iron, two-side broadband anti-reflection (AR) coated glass with 95% transmission at 0° AOI); (2) we assume a module-level 5% power loss due to lens-to-cell alignment inaccuracies (empirically determined); (3) the backplane (glass–Si–glass laminate for hybrid design, glass plate for translucent design) is two-side AR coated; (4) the efficiency of the III–V triple-junction cell is realistically assumed to be 41.5% under a concentration of 180×. The efficiency of the c-Si submodule is assumed to be 20% at Standard Test Conditions (STC), but a 3% relative loss is applied to take into account the low irradiance conditions (∼200 W/m^2) at the backplane[33]; (5) shading losses, that is, the ratio of the backplane that is covered with III–V cells and interconnections, thus preventing diffuse light to reach the Si backplane (in the hybrid system) or to be transmitted (in the translucent system), are set to 15%. These simulation parameters result in a calculated efficiency of 29% (CSTC) for the CPV part of the module, in agreement with measurement realized at concentrator STC in 2019.[11] Table 1 summarizes the locations considered for energy yield estimations: Lausanne, Madrid, Almeria, and Phoenix, along with the values of yearly irradiation and module tilt for each location. Panels are tilted due South, 10° lower than the latitude.

*The angular transmission of diffuse light is ray traced for each AOI separately. We used the same AM1.5 incident spectrum for simplicity, as it does not introduce a significant difference in the weighted average transmission through the optics.

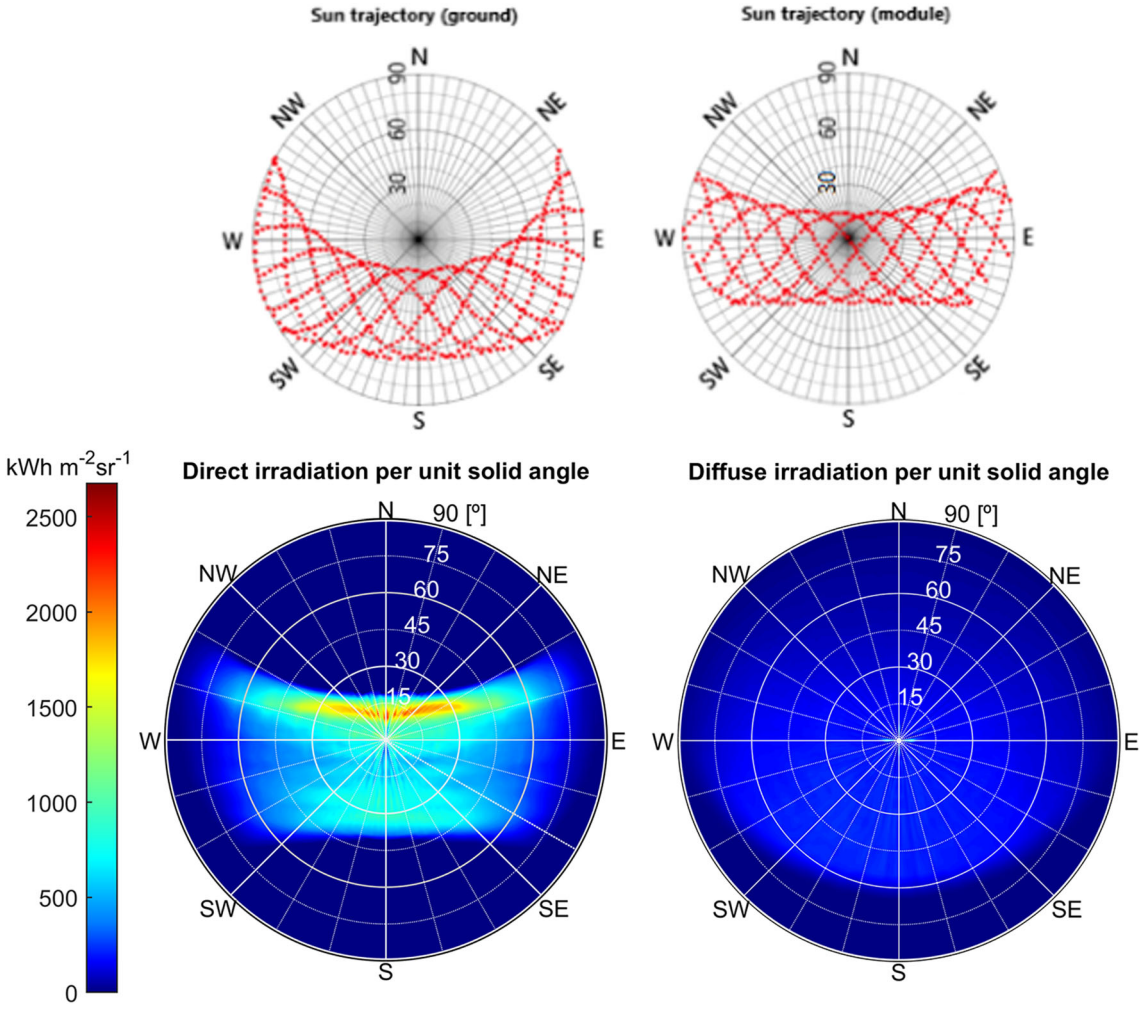

FIGURE 6 Polar plots of a sub-sample of solar positions through the year (in ground and module reference frames) (top), and angular distributions of direct and diffuse inclined irradiation per solid angle on the module plane, for Madrid and a module tilt of 30° (bottom). The solar trajectories are projected to the module reference frame so the plot radius represents the solar angle with respect to the module normal. Please note that East and West are now 90° and 270° of azimuth with respect to the north of this new reference frame. Therefore, the solar noon for summer months is north to this normal vector. Solar resource was calculated from the 2005–2016 TMY available at the PVGIS tool

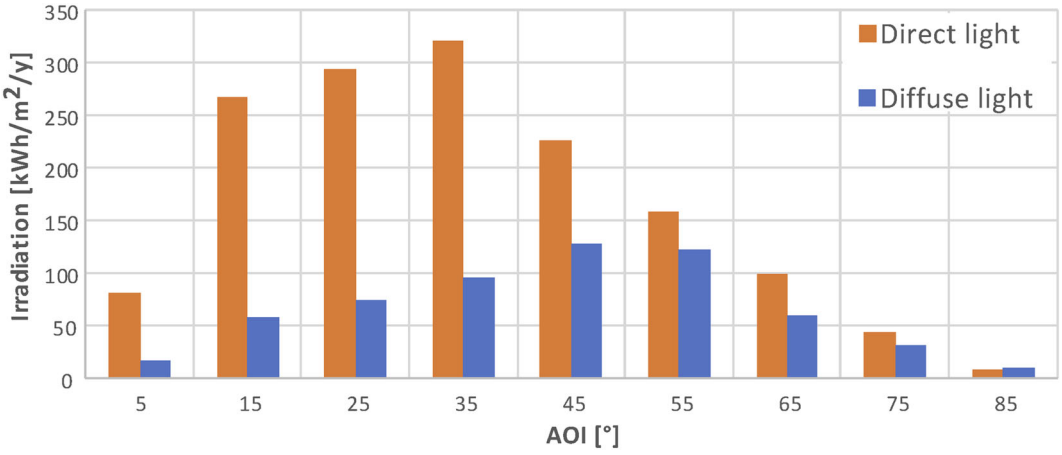

FIGURE 7 Angular distribution (10° bins) of yearly direct and diffuse inclined irradiation available in Madrid versus AOI for on a plane with a tilt of 30° due South

TABLE 1 Locations considered for energy yield estimations

Location	Latitude, longitude	Module tilt	GHI (kWh/m^2/year)	DNI (kWh/m^2/year)	DHI (kWh/m^2/year)
Lausanne	46.5°N, 6.63°E	36°	1,362.2	1,478.1	551.4
Madrid	40.42°N, 3.70°W	30°	1,812.8	2,206.8	556.9
Almeria	36.84°N, 2.46°W	27°	1,906.7	2,296.6	556.2
Phoenix	33.45°N, 112.07°W	23°	1,986.5	2,530.2	454.7

3.1.4 | Energy yield predictions for the hybrid PV-CPV system

We compare in Figure 8 the energy yield calculation results for (1) A planar micro-tracking system with III–V cells only, (2) a planar micro-tracking system with III–V cells and a backplane of generic Si cells, and (3) a generic Si module (20% efficiency). The results show that the planar tracking micro-CPV with III–V cells alone has a lower energy yield than conventional Si PV in the medium- and low-DNI locations. The two systems are almost on par in Southern Spain, and planar-tracking micro-CPV takes the advantage over conventional Si PV in high-DNI regions like Phoenix. The energy yield ratio as a function of diffuse light content (diffuse horizontal irradiance (DHI)/GHI) is shown by the gray curve in Figure 10. Remarkably, when adding a Si layer to form a hybrid III–V/Si system, planar tracking micro-CPV takes the advantage over conventional Si PV for all locations, including low-DNI Lausanne. The orange curve in Figure 10 shows an energy advantage of hybrid planar tracking micro-CPV up to 28.8% over conventional Si PV. It is interesting to look at the boost provided by the addition of the Si cells in the planar-tracking architecture (blue curve in Figure 10): the boost is always significant, (15% even in high-DNI Phoenix), although more significant in the low-DNI region (over 30% in Lausanne).

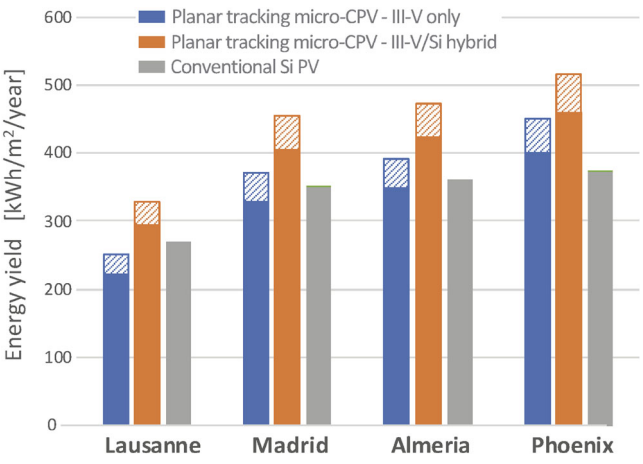

FIGURE 8 Comparison of yearly energy yield per square millimeter of module in Lausanne, Madrid, Almeria, and Phoenix for three different systems: Planar-tracking micro-CPV with III–V cells only, planar-tracking micro-CPV with hybrid III–V/Si architecture, and conventional Si PV. The plain columns are the results of calculation with current design. The dashed add-ons show a forward-looking scenario (3 years from now), based on improvements planned within the HIPERION project (but not taking into account the enhancement potential of bifacial Si cells in the hybrid architecture)

3.1.5 | Energy yield predictions for the translucent system

The energy yield of translucent modules (THEIA) is the same as for the planar-tracking micro-CPV system with III–V cells only. We also plot in Figure 9 the energy included in the PAR spectrum transmitted through the module, available for crop production. It should be noted that it scales with DHI rather than GHI. Interesting for agrivoltaics systems is the comparison of THEIA with a Si cell system whose absorbers would be spaced to let the same amount of transmitted light energy through as the diffuse light transmitted by THEIA (in the module plane). The percentage of the uncovered area in the Si system would go from 31% in Lausanne to 18% in Phoenix. The energy yield of a Si array with the coverage calculated above is plotted in Figure 9 for comparison and is always significantly lower than the energy yield of THEIA. The quantitative comparison is shown by the yellow curve in Figure 10, demonstrating an energy yield advantage for THEIA over a spaced Si array, for all locations considered and up to 30%. Also not included here, THEIA system has a functional advantage as it can be misaligned on purpose to let the direct light be transmitted through the module instead of converted into electricity, if needed for the crop production at specific times of the season or the day. This dynamic control feature may provide an advantage in ground covering ratio allowed for the THEIA installation over a static system.

3.1.6 | Planned improvements

The above prediction figures are based on the current design of Insolight modules. Further improvements are under development and planned to be implemented within 3 years in the framework of the HIPERION project (see Section 4): eliminating alignment losses (currently ~5%) thanks to industrial assembly process and simplification of the optical layer (removal of the front glass layer that causes 5% concentration losses at 0° AOI). These improvements will positively impact the performance of both the hybrid III–V/Si and the translucent modules, bringing the direct light-conversion efficiency closer to

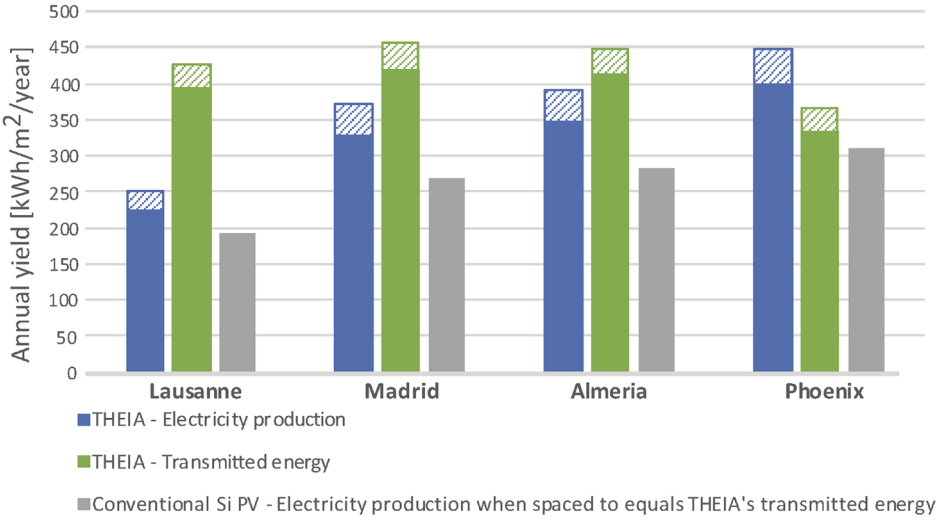

FIGURE 9 Energy yield and transmitted energy per square millimeter of module for THEIA, and comparison with a standard Si PV system whose cells are spaced to let the same amount of transmitted energy (at the module level) than THEIA. The plain columns are the results of calculation with current design. The dashed add-ons show a forward-looking scenario (3 years from now), based on improvements planned within the HIPERION project

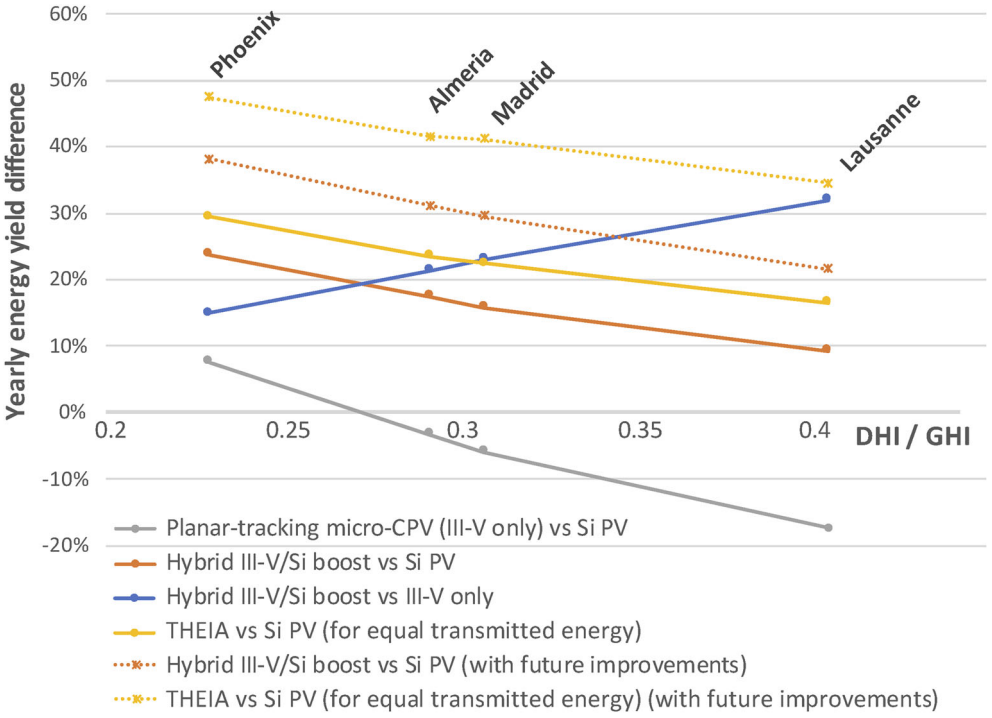

FIGURE 10 Yearly energy yield comparison for different systems. Gray: Planar tracking micro-CPV with III–V cells only compared to conventional Si PV. Orange: Hybrid III–V/Si planar tracking micro-CPV compared to conventional Si PV. Blue: Hybrid III–V/Si planar tracking micro-CPV compared to planar tracking micro-CPV with III–V cells only. Yellow: THEIA compared to a conventional Si PV array whose absorbers would be spaced to let the same amount of light transmitted than THEIA. The dotted lines show a forward-looking scenario (3 years from now), based on improvements planned within the HIPERION project

the 32% (CSTC) obtained on the lab prototype in 2016. The energy yield and comparison with standard Si PV resulting from these improvements are shown with the dashed columns in Figures 8 and 9 and with the dotted lines in Figure 10: the planar-tracking hybrid III–V/Si system will produce nearly 40% more energy than a conventional Si PV module, and the THEIA system will produce almost 50% more energy than a conventional Si PV array spaced to let the same amount of sunlight be transmitted. In addition, as mentioned in Section 2.1, Insolight hybrid architecture is optimal for the use of bifacial Si cells. The potential of bifacial boost has not been included in the above calculations, but is discussed in Section 3.3. It will further boost the performance of the hybrid III–V/Si architecture to generate up to ~30% more annual energy yield in the location studied (Madrid).

3.2 | Development of open-source models for hybrid static CPV modules on PVLIB

The modeling described in previous section is based on a methodology developed at Insolight, primarily meant to generate a good understanding of their own technology and produce sound business cases. However, it is based on a diverse toolchain, often proprietary, which cannot be easily transferred to any interested parties like investors, project engineers, or other research teams. Due to the rising interest on this hybrid CPV/PV approach, a model for this type of systems has been developed for the PVLIB Python framework. PVLIB Python is an open-source initiative supported by a large community of researchers from academia, research centers, and private companies. It provides a

library with a set of transparent and well documented classes and functions for simulating the performance of PV systems.[34] Its results have been extensively validated against other industry-standard software packages like PVSYST or SAM.[35] Its API is implemented in three layers: core functions, classes for a conventional PV system and a project location, and a class for performing a complete modeling chain. Based on the existing knowledge on the hybrid CPV/PV system by Insolight, new classes have been developed to model CPV modules (*CPVSystem*), tracking-integrated CPV modules (*StaticCPVSystem*), flat-plate submodules behind a concentrator (*StaticFlatPlateSystem*), and tracking-integrated hybrid CPV/PV modules (*StaticHybridSystem*). A hierarchical design is followed where the global *StaticHybridSystem* class is composed of the outputs of both *StaticFlatPlateSystem* and *StaticCPVSystem* classes, the latter in turn composed of the *CPVSystem* class. A diagram of the complete model is shown in Figure 11. This model can be directly fitted to the Insolight technology, but it has been conceived as a generic modeling tool for any CPV system with external or integrated tracking, hybrid or III–V alone.

In order to be as analogous as possible to PVSYST, CPV systems are modeled using the single-diode model plus two derating factors (known as utilization factors in PVSYST, *UF*) that describe additional losses produced by the sensitivity of the lens efficiency to temperature and by the nonlinear sensitivity to spectral conditions of III–V multi-junction solar cells.[36] Air mass (*AM*) and ambient temperature (T_{air}) are used as a proxy for lens temperature and spectral conditions, respectively. Each UF is a piecewise linear approximation of the nonlinear behavior of module efficiency versus those quantities. The irradiance available for static (tracking-integrated) systems is modeled by adding transposition models from DNI and GHI to direct and global irradiance at the plane of array, DII and GII, respectively. The tracking range of 55° is taken into account through the AOI_{limit} parameter, beyond which DNI is not captured by the CPV submodule anymore, but contributes to the flat-plate submodule. IAMs for the III–V and Si submodules described in the previous section are introduced as IAM_{CPV} and $IAM_{flat\ plate}$, respectively.

The model has been developed with functional and physical unit tests to check the coherence of the results. Its ability to model Insolight technology has been already explored using an outdoor measurement campaign carried out at the rooftop of the Solar Energy Institute of the UPM in Madrid.[37] The left side of Figure 12 shows the hourly comparison of the measured and modeled performance during two sample days for the two outputs of the Insolight technology: the III–V submodule (top) and the c-Si submodule (bottom). The model is able to reproduce the behavior during clear and cloudy days and the switching behavior when the tracking range is exceeded, although the model is still under validation. The root mean square error (RMSE) and mean bias error (MBE) of the modeling are given for the 2 days shown: RMSE is 1.6 and 0.34 W for the III–V and Si subsystems, respectively. Modeling errors are mostly linked to the response at the high-AOI tails.

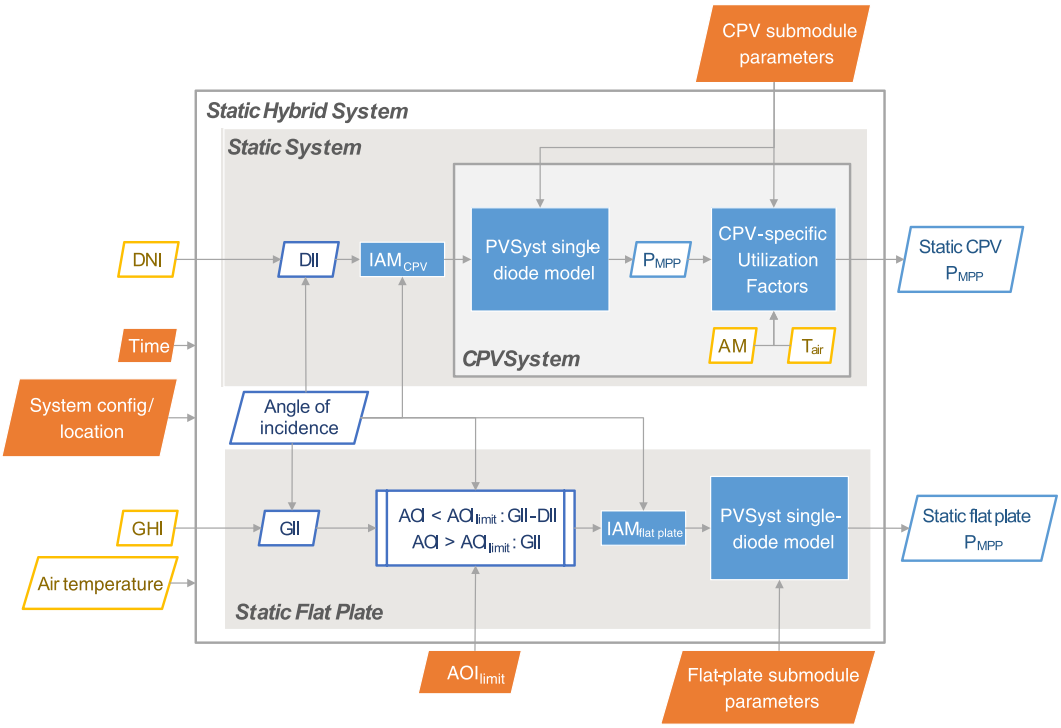

FIGURE 11 Diagram of the PVLIB classes developed to model integrated-tracking hybrid systems composed of a CPV submodule that collects direct irradiance and a flat-plate PV submodule that collects diffuse irradiance

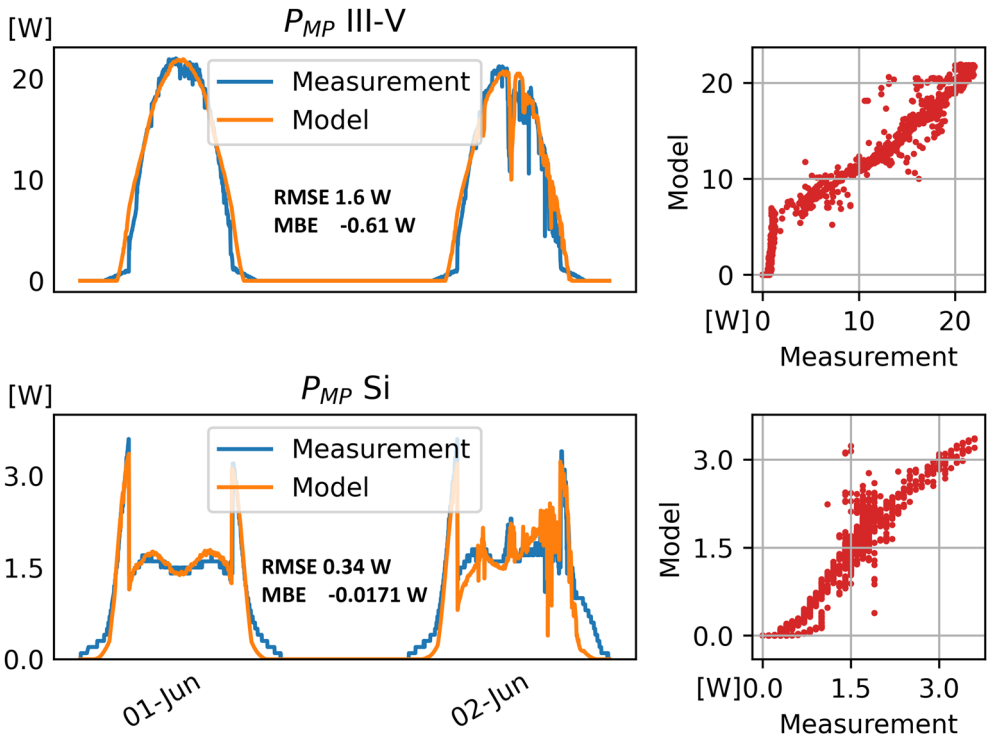

FIGURE 12 Hourly comparison of measured and modeled performance for the III–V and Si submodules within the Insolight hybrid module during two sample days: a clear sky day (June 1) and a cloudy and clear day (June 2)

3.3 | CSEM model for bifacial Si cells performance under diffuse light

All simulations of the hybrid modules presented in the previous sections only account for the front-side contribution of the silicon backplane. The backplane energy production can be increased either by covering the rear side of the module with a white backsheet or using bifacial solar cells, transforming the hybrid CPV/PV Insolight module into a bifacial device.

In the present section two bifacial configurations are considered:

- Configuration A (see Figure 13, left) consists in eight strings of eight half interdigitated back contact (IBC) solar cells with a measured bifaciality factor ϕ of 0.5.
- Configuration B (see Figure 13, right) consists in six strings of six half-cut heterojunction (HJT) solar cells with a bifaciality factor ϕ of 0.95.

Using a white backsheet helps increasing the photogenerated current as the light that hits the backsheet is diffused and can be reabsorbed by the silicon solar cells due to total internal reflection on the backplane front glass. This so-called *zero-depth concentrator effect* is interesting in the present case due to the small filling factor of the solar cells (i.e., the relative area of the solar cells to the module area). A relative gain on power of 3.3% and 4.8% was measured following this approach for configurations A and B, with filling factors of 77.6% and 73.6%, respectively. In approach A, eight strings of eight IBC bifacial half cells are interconnected in series whereas in approach B, six strings of six bifacial HJT half-cells are interconnected in series with a multi-wire approach. In the latter case, the number of interconnector has been optimized to achieve the best performance in the non-standard operating conditions, that is, about 0.3 suns of irradiance. The bifaciality factors have been estimated for each configuration as the ratio of

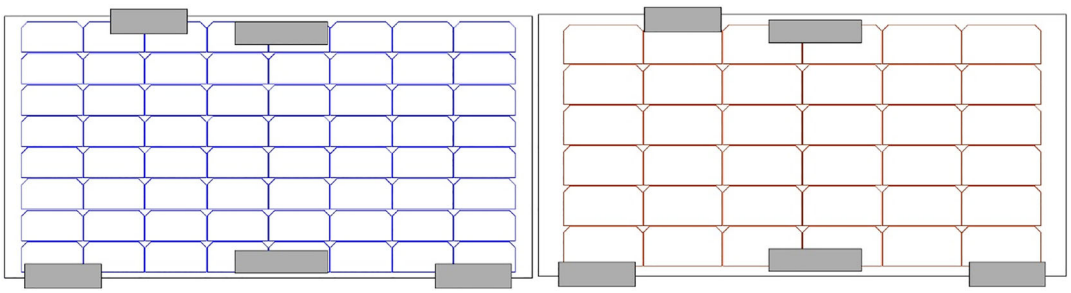

FIGURE 13 Left: configuration A with eight strings of eight half-cut IBC solar cells. Cells are connected in series along the long dimension. Right: configuration B with six strings of six half-cut HJT solar cells. Cells are connected in series along the small dimension. The gray rectangles are module components inducing shading on the rear side of the Si cells. Each string is connected in parallel with a bypass diode

rear and front short-circuit current (I_{SC}) measured on each module side after removal of the PCB permanent shading.

Energy gains associated to bifaciality will be larger than in conventional flat plate because the front side only receives the diffuse fraction further shaded by the optics and III–V arrays. In contrast, the rear side is only shaded by some small actuation elements (highlighted with gray boxes in Figure 13) and will receive most of the incident irradiance reflected from the terrain and surroundings. To reduce the mismatch losses that these actuation elements introduce, each string is connected in parallel with a bypass diode. Thus, the role of bypass diodes is important and has been included in the modeling below.

Irradiance received at the rear plane critically depends on the characteristics of the surroundings and mounting geometry such as ground albedo, obstacle shading, module tilt, ground clearance or array spacing. The main parameters affecting the bifacial energy gain are ground albedo (the fraction of irradiance incident on the terrain that is reflected in backscattering) and ground clearance, namely, the distance between the ground and the bottom of the module frame. Clearance impacts the view factor of the module rear surface, increasing the amount of effective irradiance absorbed by the module.

Energy yield and bifacial gain have been simulated for configurations A and B using the Matlab PVLIB Toolbox for estimating effective in-plane irradiance.[38] To properly account for the effect of non-uniform irradiance, a Matlab procedure developed at CSEM calculates the full module IV curve including current mismatch between cells and the effect of bypass diodes. One IV curve is calculated at each time step to improve the accuracy of the energy yield estimation. This approach allows to determine the impact of ground clearance and bypass diodes on the energy yield.

In Figure 14, three cases are considered. The first one corresponds to a standard installation where the module is directly installed on a flat rooftop with a fixed tilt angle and a zero ground clearance. The second case could correspond to a bifacial rack structure (50-cm clearance) in a utility-scale power plant or a large industrial rooftop system, and the last case would correspond to a public use with 300-cm clearance (parking lot, bay window in a shopping mall, etc.). The bifacial gain rapidly increases with ground clearance until a height of 1 m and then saturates before decreasing again.[39] The reason is that the view factor of each individual cell increases with module elevation. This gain is further enhanced by the reduction of current mismatch between cells as the irradiance homogeneity from albedo is increased. This effect is visible in Figure 14 (bottom) where the irradiance hitting the rear of each individual cell is plotted for each time of the day.

The effect of bypass diodes is shown in Figure 15, where the power–voltage curve for three IBC configurations is plotted. Power is normalized to the maximum power (P_{mpp}) of the monofacial configuration estimated for clear sky conditions in Madrid at the solar noon of June 21 using Ineichen model.[40] Bifacial configurations are simulated with a ground clearance of 300 cm. For the simulations, the front irradiance is composed of the direct, sky-diffused, and ground-reflected components. The rear irradiance is composed of the ground-reflected and sky-diffuse components. Under these conditions, the P_{mpp} developed by the bifacial configuration with no bypass diode is more than twice as high as the monofacial configuration. With the use of one bypass diode per string, the power gain rises to 2.5. To avoid losing too much of the bifacial gain due to mechanical elements on the module backside, bypass diodes have been integrated within the laminate.

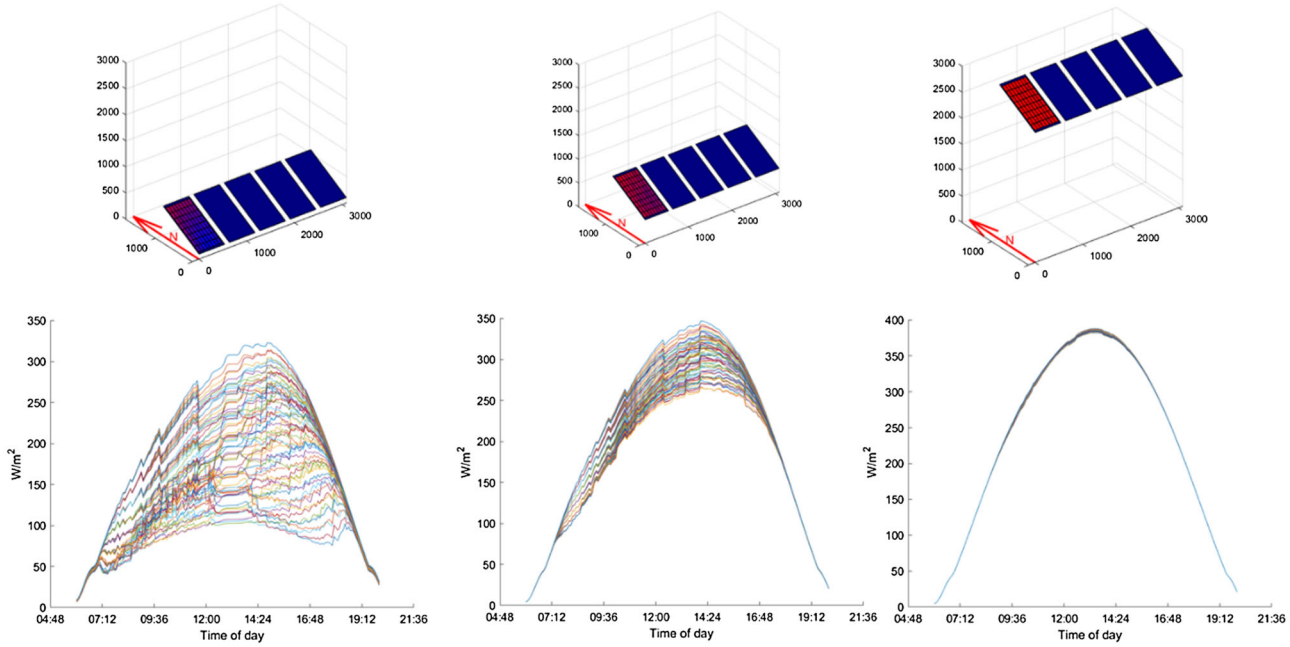

FIGURE 14 Top: colormap of the simulated irradiance reaching each cell on the rear side for three different ground clearance—0, 50, and 300 cm. Bottom: rear irradiance reaching the cells during a day under clear sky conditions (Ineichen model). Each line represents a unique cell

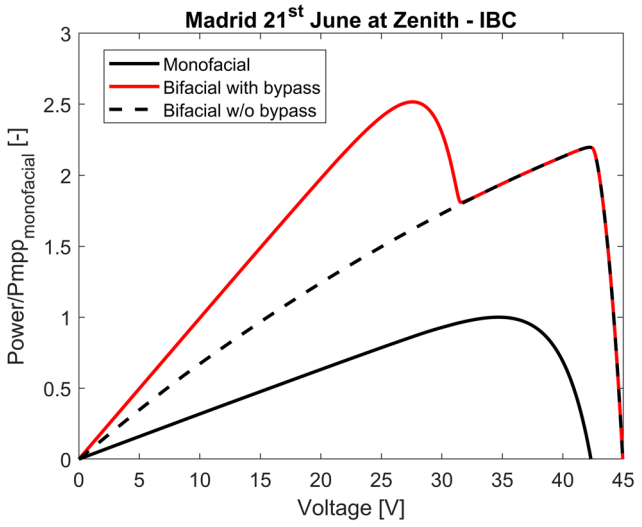

FIGURE 15 Power plot normalized by the P_{mpp} in monofacial configuration. Simulation uses synthetic clear sky conditions (Ineichen model) on June 21 at zenith time and for a 300-cm ground clearance

To calculate the bifacial gain of each configuration, the rear irradiance on each individual cell has been calculated using the view factor approach.[41,42] The TMY data from the PVGIS tool[31] were used for the yearly energy yield simulations, using the 2006–2015 period. The Perez sky diffuse model[43] was used to transpose in-plane diffuse irradiance.

The simulations presented hereafter have been performed for the first module of a row of five, considering a module spacing of 10 cm (see Figure 14). The tilt angle θ has been set according to the rule-of-thumb of the latitude −10°. For all locations, the ground albedo has been set to 0.45, corresponding to ordinary Portland cement concrete.[44] The installation is facing south (azimuth angle of 180°).

The effective irradiance G_{eff} on each individual cell at each time step is calculated as follows.

$$G_{eff} = G_{eff,rear} + G_{eff,front,diffuse} + G_{eff,front,direct}, \quad (1)$$

$$G_{eff,rear} = G_{calc,rear} \cdot (1 - Loss_{rear}) \cdot \phi_{Isc}, \quad (2)$$

$$G_{eff,front,diffuse} = G_{calc,front,diffuse} \cdot (1 - Loss_{front,diffuse}), \quad (3)$$

$$G_{eff,front,direct} = G_{calc,front,direct} \cdot (1 - Loss_{front,direct}), \quad (4)$$

where $G_{calc,rear}$, $G_{calc,front,diffuse}$, and $G_{calc,front,direct}$ are respectively the rear-side total irradiance, the front-side diffuse irradiance, and the front-side direct irradiance. ϕ_{Isc} is the measured bifaciality factor of the cell, that is, 0.5 for the IBC cell and 0.95 for the HJT cell. The *Loss* terms contain all optical contributions to irradiance for each side and each component, that is, "direct" and "diffuse":

- The term $Loss_{rear}$ encompasses the cell-dependent permanent shading at the backside and the encapsulant/glass layers losses (∼1.5%).
- The term $Loss_{front,diffuse}$ corresponds to diffuse irradiance losses due to the transmission through the lens layer (26%, a weighted average of the angular response), the shading due to PCB traces of the III–V circuit (15%) and the reflection and absorption losses at the encapsulant–glass multi-layers (2.5%).
- The term $Loss_{front,direct}$ accounts for the angular-dependent transmission losses produced on the direct beam by the front layers, as described by the IAM (see Figure 5). The static shading of PCB traces is 15%, and the encapsulant/glass multi-layers losses are 2.5% (reflection and absorption). Furthermore, $Loss_{front,direct}$ is set to 0 when the AOI of the direct beam is within the range of the CPV tracking system (±55°) as the direct beam does not reach the Si cells ideally (although in the real system this can be a mechanism for mitigation of direct light losses in case of tracking misalignment). The other angle losses are considered via the angle modifier function, measured on modules of the same technology.

The temperature of the backplane has been calculated using the model given in the IEC 61853-2 standard where the module temperature depends on the irradiance (*G*), the ambient temperature (T_{amb}) and the wind speed (v_{wind}) according to relation 5:

$$T_{mod} - T_{amb} = \frac{G}{u_0 + u_1 \cdot v_{wind}}, \quad (5)$$

where G is the irradiance, the coefficient u_0 describes the irradiance influence and the u_1 the wind influence. This empirical model is assumed to be valid in the present bifacial hybrid design, but this assumption requires further demonstration.

For the interconnection simulation, each cell is defined by a two-diode model, the effective irradiance and the backplane temperature. This cell-level approach allows considering the mismatch losses due to the different effective irradiances and evaluating the impact of the module elevation as well as the shading of components on the back side of the module. The simulation is performed by interconnecting all the cells in series and each string in parallel with a bypass diode.

The bifacial gain $Bifi_{gain}$ is calculated using relation 6:

$$Bifi_{gain} = \frac{(E_{bifacial} - E_{monofacial})}{E_{monofacial}}, \quad (6)$$

where *E* stands for the yearly energy yield. Please note that this bifacial gain will be higher than in bare flat-plate modules because only the diffuse fraction is collected at the front side (the one driving $E_{monofacial}$).

In Figure 16, $Bifi_{gain}$ has been computed for the two types of bifacial configurations A (IBC) and B (HJT) simulated to be in Madrid under three different clearance heights. The energy gain using bifacial configurations for the Si backplane is obvious. The bifacial gain goes

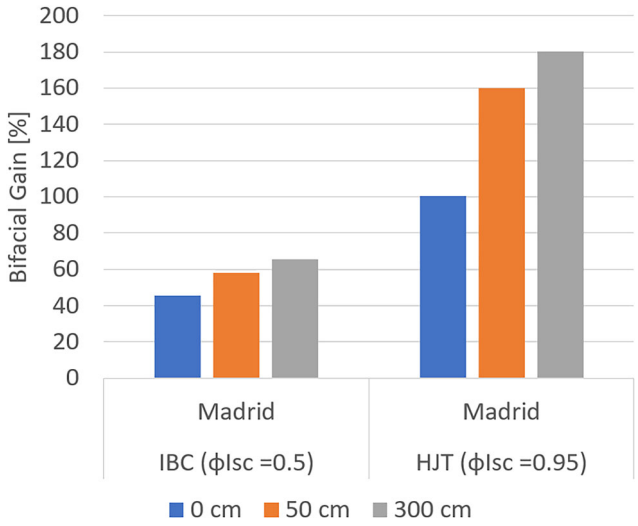

FIGURE 16 Estimated bifacial gains on the yearly energy yield for configurations A and B in Madrid at three different ground clearance heights. Please note that the front side receives diffuse irradiance only. For comparison, 40% bifacial gain is obtained in the 50-cm-clearance simulation setup for bare flat-plate HJT modules (without the CPV cover)

from 45.7% in Madrid for IBC cells with low clearance (rooftop mounted) to 180% for a high clearance of 300 cm using HJT cells. The lower gains of IBC are linked to their lower bifaciality, limited by the back contact shading, and the larger shading factor of single strings produced by the positioning components as evidenced in Figure 13. In the best scenarios given above, a bifacial boost of 160%–180% on the c-Si layer of the hybrid architecture will boost the yearly energy yield calculated in Section 3.1 of the hybrid planar tracking micro-concentrator module by ~30%.

These unusually high bifacial gains are explained by the respective contributions of front and rear sides on the effective irradiance. Contrary to conventional bifacial modules, the front side only receives the diffuse fraction which is further lowered by the optical layer and the III–V primary cells array. On the rear side, the irradiance reaching the backplane does not significantly differ from a conventional bifacial module, except for the static shading elements. This configuration leads to a smaller contribution of the front compared to the rear side to the effective irradiance. This asymmetry is further enhanced for the HJT case due to the higher bifaciality. For comparison, the HJT configuration has been simulated in the standard case (i.e., without the optics and primary cells stacks) in Madrid for a 50-cm ground clearance yielding a bifacial gain of 40%.

4 | ROADMAP TO INDUSTRIAL PRODUCTION

The key components of Insolight modules have already been extensively validated:

- Multi-junction solar cells have been used for many years in terrestrial and space applications (satellites) demonstrating reliable performance at high concentration with very low degradation rates and mean time to failure higher than 30 years.[45–47]
- The optical layer is made of optical silicone or solar-grade PMMA, materials that have also been qualified for photovoltaic applications, enduring extended exposure to UV radiation, humidity, and high ambient temperature.[48–50] The lens clusters are manufactured by injection molding, a low-cost industrial process with high throughput and good repeatability.
- The specific model of electrical actuators used for the micro-tracking feature have been developed and qualified for the automotive industry in high duty-cycle applications. They have a high Ingress Protection rating (IP6K9K) ensuring protection against water or dust ingress.

As detailed in Section 2, multiple performance and reliability demonstrations have also been performed at module level on multiple prototype of various sizes ranging from 0.1 to 0.6 m^2, among which some modules installed and monitored at EPFL (Lausanne, Switzerland) since 2017.

On the road to commercialization, the main challenges that remain are therefore not at component-level, but rather in the selection of the proper industrial processes required to assemble these modules in a cost-effective manner, without compromising on performance or reliability. For instance, the selection of an adhesive and deposition process to ensure an accurate positioning and stable bonding of the optical layer to the protective glass cover or the selection and printing of a stable high-conductivity paste on glass for the interconnection of multi-junction solar cells.

While the existing Insolight prototypes have been assembled using semi-manual processes in a lab environment, the goal of the HIPERION project is to develop a pilot production line demonstrating the industrial feasibility, throughput and repeatability of all the key module assembly steps. This is done in several phases, first by assembling a pre-series of modules in 2020 using non-optimized equipment, then by developing dedicated high-throughput machines which will be operational in the second half of 2021. The transition to industrial assembly processes also offers potential for performance improvements, as high-precision automated cells and optics positioning can reduce alignment losses in comparison to the semi-manual processes used up to now.

Another challenge that the HIPERION consortium aims to solve lies in the proper characterization and power rating of these modules. Due to their specific architecture and unique features, the modules cannot be measured and rated in the exact same manner as conventional silicon PV modules. For instance, a light beam with a high degree of collimation (half-angle in the range of 0.3°) and a broad spectrum (300 to 1,800 nm) is required for the characterization of the III–V submodule. Moreover, existing industry norms do not encompass hybrid modules, capable of collecting both direct and diffuse sunlight with two different types of solar cells. Defining a proper

methodology to rate the nominal power of such modules is therefore another goal of HIPERION.

5 | CONCLUSIONS

We have presented a micro-CPV module architecture with integrated planar tracking that can be installed at a fixed tilt in a static frame. The concept combines the high-efficiency of CPV (29% module efficiency on direct sunlight at CSTC) with the ease of installation of standard flat-plate PV. Two hybrid architectures have been presented to harvest the diffuse component of solar irradiance: (1) a hybrid architecture where diffuse light is harvested by a layer of Si cells; (2) a translucent architecture where diffuse light is transmitted through the module for dual-land-use applications, such as agrivoltaics. We have presented a set of simulation results that predict energy yields for the hybrid and translucent architecture and compared it to a reference 20% efficiency flat-plate PV.

The results show that the hybrid architecture provides an excess of yearly energy production compared to the reference flat-plate PV system in all locations studied, including those with a low-DNI content, and up to 38% advantage in high-DNI locations. Therefore, rooftop markets in most of Europe are enabled, where self-consumption at a levelized cost of electricity below the grid prices can ultimately provide economic benefits over conventional Si PV. The hybrid architecture backplane is based on a standard glass–Si–glass laminate that is directly compatible with bifacial Si cells, and we calculate the additional energy production generated for different types of cells and ground clearance heights. The translucent architecture can provide up to 47% excess electricity compared to a reference Si array that would be spaced to transmit the same amount of solar PAR for crop production. Additionally, planar tracking of translucent modules can be used to produce dynamic control of sunlight to optimize the radiation doses required to maximize crop yields. An open-source modeling toolbox is being developed within the PVLIB framework and shows a good ability to reproduce the performance of the hybrid architecture. The ongoing H2020 HIPERION project is tackling the challenges of mass production, with a pilot high-throughput production line to be completed by 2021, bringing the planar tracking micro-CPV modules one step closer to commercialization.

ACKNOWLEDGEMENTS

This work has received funding from the European Union's Horizon 2020 research and innovation program under Grant Agreement n°857775 (project HIPERION) and under Grant Agreement n°787289 (project GRECO), the Eurostars Program (MEPV-2 project), and from Innosuisse (Swiss Innovation Agency)—Helios project.

ORCID

César Domínguez https://orcid.org/0000-0002-2751-7208
Stephen Askins https://orcid.org/0000-0002-9988-2917
Rubén Núñez https://orcid.org/0000-0001-9160-5416
Norman Jost https://orcid.org/0000-0002-0111-9498
Guido Vallerotto https://orcid.org/0000-0002-5266-6491
Ignacio Antón https://orcid.org/0000-0002-6890-5477

REFERENCES

1. Steiner M, Siefer G, Schmidt T, Wiesenfarth M, Dimroth F, Bett AW. 43% sunlight to electricity conversion efficiency using CPV. *IEEE J Photovolt*. 2016;6(4):1020-1024.
2. Wiesenfarth M, Philipps SP, Bett AW, Horowitz K, Kurtz S. Current status of concentrator photovoltaic (CPV) technology—Fraunhofer ISE. Fraunhofer Institute for Solar Energy Systems ISE, National Renewable Energy Laboratory NREL; 2017. Accessed May 12, 2019. https://www.ise.fraunhofer.de/en/publications/studies/studie-current-status-of-concentrator-photovoltaic-cpv-technology.html
3. Nielson GN, Okandan M, Resnick P, et al. Microscale c-Si (c)PV cells for low-cost power. In: 2009 34th IEEE Photovoltaic Specialists Conference (PVSC). 2009:001816-001821. https://doi.org/10.1109/PVSC.2009.5411500
4. Apostoleris H, Stefancich M, Chiesa M. Tracking-integrated systems for concentrating photovoltaics. *Nat Energy*. 2016;1(4):16018. https://doi.org/10.1038/nenergy.2016.18
5. Martínez JF, Steiner M, Wiesenfarth M, Dimroth F. 4-Terminal CPV module capable of converting global normal irradiance into electricity. *AIP Conf Proc*. 2018;2012(1):090005. https://doi.org/10.1063/1.5053543
6. Duerr F, Meuret Y, Thienpont H. Tracking integration in concentrating photovoltaics using laterally moving optics. *Opt Express*. 2011;19(103):A207-A218. https://doi.org/10.1364/OE.19.00A207
7. Lim T, Kwak P, Song K, Kim N, Lee J. Automated dual-axis planar solar tracker with controllable vertical displacement for concentrating solar microcell arrays. *Prog Photovolt Res Appl*. 2017;25(1):123-131. https://doi.org/10.1002/pip.2843
8. Ito A, Sato D, Yamada N. Optical design and demonstration of micro-tracking CPV module with bi-convex aspheric lens array. *Opt Express*. 2018;26(18):A879-A891. https://doi.org/10.1364/OE.26.00A879
9. Chinello E, Modestino MA, Schüttauf JW, et al. A comparative performance analysis of stand-alone, off-grid solar-powered sodium hypochlorite generators. *RSC Adv*. 2019;9(25):14432-14442. https://doi.org/10.1039/C9RA02221J
10. Nardin G, Aguilar AF, Anglade L, et al. Towards industrialization of planar microtracking photovoltaic panels. *AIP Conf Proc*. 2019;2149(1):040001. https://doi.org/10.1063/1.5124185
11. Askins S, Jost N, Aguilar AF, et al. Performance of hybrid micro-concentrator module with integrated planar tracking and diffuse light collection. In: 2019 IEEE 46th Photovoltaic Specialists Conference (PVSC); 2019:2507-2512. https://doi.org/10.1109/PVSC40753.2019.8980519
12. Haney MW, Gu T, Agrawal G. Hybrid micro-scale CPV/PV architecture. In: 2014 IEEE 40th Photovoltaic Specialist Conference (PVSC); 2014:2122-2126. https://doi.org/10.1109/PVSC.2014.6925343
13. Vivar M, Herrero R, Anton I, et al. Effect of soiling in CPV systems. *Sol Energy*. 2010;84(7):1327-1335.
14. Lee K-T, Yao Y, He J, et al. Concentrator photovoltaic module architectures with capabilities for capture and conversion of full global solar radiation. *Proc Natl Acad Sci U S a*. 2016;113(51):E8210-E8218. https://doi.org/10.1073/pnas.1617391113
15. Sato D, Yamada N, Lee K-H, Araki K, Yamaguchi M. Design and evaluation of partial concentration III–V/Si module with enhanced diffuse sunlight transmission. In: 2017 IEEE 44th Photovoltaic Specialist Conference (PVSC); 2017:1743-1746. https://doi.org/10.1109/PVSC.2017.8366603
16. Yamada N, Hirai D. Maximization of conversion efficiency based on global normal irradiance using hybrid concentrator photovoltaic architecture. *Prog Photovolt Res Appl*. 2016;24(6):846-854. https://doi.org/10.1002/pip.2765

17. Martínez JF, Steiner M, Wiesenfarth M, et al. Development and outdoor characterization of a hybrid bifacial HCPV module. *Prog Photovolt Res Appl*. 2020;28(5):349-357. https://doi.org/10.1002/pip.3239
18. Gu T, Li D, Li L, et al. Wafer-level integrated micro-concentrating photovoltaics. In: *Light, Energy and the Environment (2016), Paper PTh3A.1*. Optical Society of America; 2016:PTh3A.1. https://doi.org/10.1364/PV.2016.PTh3A.1
19. Hirai D, Okamoto K, Yamada N. Fabrication of highly transparent concentrator photovoltaic module for efficient dual land use in middle DNI region. In: 2015 *IEEE 42nd Photovoltaic Specialist Conference (PVSC)*. 2015:1-4. https://doi.org/10.1109/PVSC.2015.7355759
20. Sato D, Yamada N. Design and testing of highly transparent concentrator photovoltaic modules for efficient dual-land-use applications. *Energy Sci Eng*. 2020;8(3):779-788. https://doi.org/10.1002/ese3.550
21. Fraunhofer ISE. Harvesting the sun for power and produce—agrophotovoltaics increases the land use efficiency by over 60 Percent. Published online 2017. Accessed July 6, 2020. https://www.ise.fraunhofer.de/en/press-media/press-releases/2017/harvesting-the-sun-for-power-and-produce-agrophotovoltaics-increases-the-land-use-efficiency-by-over-60-percent.html
22. Barron-Gafford GA, Pavao-Zuckerman MA, Minor RL, et al. Agrivoltaics provide mutual benefits across the food–energy–water nexus in drylands. *Nat Sustain*. 2019;2(9):848-855. https://doi.org/10.1038/s41893-019-0364-5
23. Dupraz C, Talbot G, Marrou H, et al. To mix or not to mix: evidences for the unexpected high productivity of new complex agrivoltaic and agroforestry systems. In: Proceedings of the 5th World Congress of Conservation Agriculture: Resilient Food Systems for a Changing World. 2011.
24. Weselek A, Ehmann A, Zikeli S, Lewandowski I, Schindele S, Högy P. Agrophotovoltaic systems: applications, challenges, and opportunities. A review. *Agron Sustain Dev*. 2019;39(4):1-20. https://doi.org/10.1007/s13593-019-0581-3
25. Schindele S, Trommsdorff M, Schlaak A, et al. Implementation of agrophotovoltaics: Techno-economic analysis of the price-performance ratio and its policy implications. *Appl Energy*. 2020;265:114737. https://doi.org/10.1016/j.apenergy.2020.114737
26. Cossu M, Yano A, Li Z, et al. Advances on the semi-transparent modules based on micro solar cells: first integration in a greenhouse system. *Appl Energy*. 2016;162:1042-1051. https://doi.org/10.1016/j.apenergy.2015.11.002
27. Li Z, Yano A, Cossu M, Yoshioka H, Kita I, Ibaraki Y. Shading and electric performance of a prototype greenhouse blind system based on semi-transparent photovoltaic technology. *J Agric Meteorol*. 2018;74(3):114-122. https://doi.org/10.2480/agrmet.D-17-00047
28. Loik ME, Carter SA, Alers G, et al. Wavelength-selective solar photovoltaic systems: powering greenhouses for plant growth at the food–energy–water nexus. *Earths Future*. 2017;5(10):1044-1053. https://doi.org/10.1002/2016EF000531
29. Valle B, Simonneau T, Sourd F, et al. Increasing the total productivity of a land by combining mobile photovoltaic panels and food crops. *Appl Energy*. 2017;206:1495-1507. https://doi.org/10.1016/j.apenergy.2017.09.113
30. Apostoleris H, Chiesa M. High-concentration photovoltaics for dual-use with agriculture. *AIP Conf Proc*. 2019;2149(1):1-5, 050002. https://doi.org/10.1063/1.5124187
31. Huld T, Müller R, Gambardella A. A new solar radiation database for estimating PV performance in Europe and Africa. *Sol Energy*. 2012;86(6):1803-1815. https://doi.org/10.1016/j.solener.2012.03.006
32. Darula S, Kittler R. CIE general sky standard defining luminance distributions. *Proc ESim* Published online. 2002;11-13.
33. Mavromatakis F, Vignola F, Marion B. Low irradiance losses of photovoltaic modules. *Sol Energy*. 2017;157:496-506. https://doi.org/10.1016/j.solener.2017.08.062
34. Holmgren WF, Hansen CW, Mikofski MA. pvlib python: a python package for modeling solar energy systems. *J Open Source Softw*. 2018;3(29):884. https://doi.org/10.21105/joss.00884
35. Gurupira T, Rix A. PV simulation software comparisons: PVSYST, NREL SAM and PVLIB. In: Conf.: SAUPEC.; 2017.
36. Gerstmaier T, van Riesen S, Gombert A, Mermoud A, Lejeune T, Duminil E. Software modeling of FLATCON© CPV Ssystems. In: *AIP Conference Proceedings*. Vol 1277. AIP Publishing; 2010:183-186. https://doi.org/10.1063/1.3509185
37. Askins S, Nardin G, Ackermann M, Gerlich F, Dominguez C. Outdoor monitoring of a hybrid micro-CPV solar panel with integrated micro-tracking and diffuse capture (Version v1.0) [Data set]. Published online July 23, 2019. https://doi.org/10.5281/zenodo.3346823
38. Stein JS, Holmgren WF, Forbess J, Hansen CW. PVLIB: open source photovoltaic performance modeling functions for Matlab and Python. In: 2016 IEEE 43rd Photovoltaic Specialists Conference (PVSC); 2016:3425-3430. https://doi.org/10.1109/PVSC.2016.7750303
39. Yusufoglu UA, Pletzer TM, Koduvelikulathu LJ, Comparotto C, Kopecek R, Kurz H. Analysis of the annual performance of bifacial modules and optimization methods. *IEEE J Photovolt*. 2015;5(1):320-328. https://doi.org/10.1109/JPHOTOV.2014.2364406
40. Ineichen P, Perez R. A new airmass independent formulation for the Linke turbidity coefficient. *Sol Energy*. 2002;73(3):151-157. https://doi.org/10.1016/S0038-092X(02)00045-2
41. Yusufoglu UA, Lee TH, Pletzer TM, et al. Simulation of energy production by bifacial modules with revision of ground reflection. *Energy Procedia*. 2014;55:389-395. https://doi.org/10.1016/j.egypro.2014.08.111
42. Cengel YA, Ghajar AJ. Radiation heat transfer. In: *Heat Transfer: A Practical Approach*. 2nd ed. McGraw-Hill; 2003:605-666.
43. Perez R, Ineichen P, Seals R, Michalsky J, Stewart R. Modeling daylight availability and irradiance components from direct and global irradiance. *Sol Energy*. 1990;44(5):271-289. https://doi.org/10.1016/0038-092X(90)90055-H
44. Kaloush KE, Carlson JD, Golden JS, Phelan PE. The thermal and radiative characteristics of concrete pavements in mitigating urban heat island effects; 2008:139p. Accessed July 6, 2020. https://trid.trb.org/view/876559
45. Algora C. Reliability of III–V concentrator solar cells. *Microelectron Reliab*. 2010;50(9–11):1193-1198.
46. Muller M, Jordan D, Kurtz S. Degradation analysis of a CPV module after six years on-sun. 2015;1679:020004. https://doi.org/10.1063/1.4931504
47. Wüllner J, Steiner M, Wiesenfarth M, Bett AW. Operation & maintenance—the key for reliable performance in a CPV power plant. In: 2018:020011. https://doi.org/10.1063/1.5053499
48. Miller DC, Khonkar HI, Herrero R, et al. An end of service life assessment of PMMA lenses from veteran concentrator photovoltaic systems. *Sol Energy Mater sol Cells*. 2017;167:7-21. https://doi.org/10.1016/j.solmat.2017.03.031
49. Miller DC, Kurtz SR. Durability of Fresnel lenses: a review specific to the concentrating photovoltaic application. *Sol Energy Mater Sol Cells*. 2011;95(8):2037-2068. https://doi.org/10.1016/j.solmat.2011.01.031
50. De Buyl F, Beukema M, Tiggelen K, Rong KW, Rankey NL, Steinbrecher J. Dow corning moldable silicone leading innovation in LED light fixtures. *J Soc Silicon Chem*. 2014;31:23-38.

How to cite this article: Nardin G, Domínguez C, Aguilar ÁF, et al. Industrialization of hybrid Si/III–V and translucent planar micro-tracking modules. *Prog Photovolt Res Appl*. 2020;1–16. https://doi.org/10.1002/pip.3387